Supporting Information

Pai et al. 10.1073/pnas.1211072109

SI Text

1. Construction of Plasmids. ***1.1 pExo.*** Construction of BlaMs (Fig. S1*A*) was based on the works by Chervaux et al. (1) and Tzschaschel et al. (2). An intermediate plasmid, pBlaM, was constructed by PCR-amplifying *bla* gene from pSND-1 without the first 66 bp and inserting it under $P_{lac/ara-1}$ of pPROLar.A122 (Clontech). The first 66-bp code for the periplasmic location peptide and its removal makes BlaM cytoplasmic in contrast to WT Bla (3). A start codon (atg) for the truncated *bla* was included during the PCR, resulting in *blaM*. Effective N-terminal sequence of *blaM* is –ATG*CACCCAGAAACG..., where the asterisk indicates the position of the sequence that is removed. The inducible expression and β-lactamase activity of the cytoplasmic BlaM in plasmid pBlaM was first tested and confirmed. BlaMs, the secretion-proficient protein, was designed from *blaM* and hemolysin secretion signal tag *hlyAs* from the *hlyA* gene using fusion PCR (1–5). Plasmid pBlaM was used as the template for the BlaM part (primers 1 and 3). The *hlyA* signal tag was PCR-amplified (primers 2 and 4) from the *hlyA* containing plasmid pLG612-1b (gift from Barbara Tzschaschel) (2). The two fragments were combined using primers 1 and 4, and the fusion gene was cloned in the pPROlar.A122 vector using KpnI and BamHI digestion to give pExo coding BlaMs under $P_{lac/ara-1}$.

Primer 1: c*gggtacc*cATGcacccagaaacgctggtgaaag
Primer 2: cctcactgattaagcattggcatcccgggggaaattctcttgcaaaaaatgtatt
Primer 3 (reverse complement of primer 2): aatacatttttgcaagagaatttcccccgggatgccaatgcttaatcagtgagg
Primer 4: gc*ggatcc*ttatgctgatgctgtcaaagt

1.2. pExoI. This plasmid consists of two parts coding for BlaMs under P_{LuxI} and LuxI under $P_{lac/ara-1}$. Fragment for P_{LuxI}-controlled BlaMs was constructed using fusion PCR with aatII sites at both ends. Plasmid pluxGFPuv (6), where GFPuv is under P_{LuxI} control, was used as a template (primers 1 and 3) for the *lux* box. pExo (primers 2 and 4) was used as the template for the BlaMs gene.

Primer 1: cgaacgc*gacgtc*agtcctttgattctaataaattggatttttgtcac
Primer 2: gtcgaataaacgcaagggaggttggtatgcacccagaaacgctggtgaaag
Primer 3: ctttcaccagcgtttctgggtgcataccaacctcccttgcgtttattcgac
Primer 4: ctctct*gacgtc*ttatgctgatgctgtcaaagt

The two fragments were combined using primers 1 and 4, and they were cloned into the aatII site of pluxRI (7), giving pExoRI. pExoI was then obtained by deleting the LuxR gene (digestion with EcoRI and BamHI followed by blunting and ligation).

1.3. pRTransp. This plasmid expresses LuxR and the transporter genes HlyB and HlyD under the control of $P_{LtetO-1}$, and it was constructed using pPROTetE (Clontech). For tight, low expression of these genes, the repressor tetR transcribed constitutively from a P_{lacIq} promoter was included at the single aatII site (JM109 does not natively carry the repressor tetR). NotI-digested fragment from pVDL9.3 (2) carrying the transporter genes and KpnI-BamHI–digested LuxR from pluxRI were inserted sequentially.

2. BlaMs Secretion and Function. BlaMs is cytoplasmic but can be secreted into the extracellular medium by hemolysin transport proteins HlyB and HlyD (1) (Fig. S1*A*). When cytoplasmic, the enzyme offers no protection to β-lactam antibiotics, such as 6-aminopenicillanic acid (6-APA), which target penicillin binding proteins in the periplasm (3, 8). We verified this property using a GFP reporter under the control of PampC (9), which is induced as a result of bacterial cell wall damage caused by 6-APA action (Fig. S1*B*). We compared the protection against 6-APA provided by BlaMs (Fig. S1*B*, *Upper*) with the protection by WT Bla (Fig. S1*B*, *Lower*). These experiments were performed as follows: JM109 cells carrying P_{ampC} reporter and either pExo or pBla were diluted 10^3-fold in fresh 10 g tryptone and 7 g KCl buffered with 100 mM 3-(*N*-morpholino) propanesulfonic acid and Mops (TBK) media with or without isopropyl β-D-thiogalactoside (IPTG) after overnight growth. After raw OD reached ~0.06 (about 5 h), 25 μg/mL 6-APA were added. Samples were taken 4 h after 6-APA treatment and subject to flow cytometry analysis.

When secreted into the extracellular space by hemolysin transport proteins HlyB and HlyD, BlaMs can degrade β-lactam antibiotics and permit bacterial growth (1, 3) (Fig. S1 *C* and *D*). To confirm this result, we extracted the supernatant of cells carrying pExo in the presence or absence of transporter pVDL9.3 grown at 37 °C in LB in the presence of 1 mM IPTG. To extract supernatant, 1–2 mL culture were centrifuged, and supernatant was then filtered using a sterile syringe filter with 0.2-μm cellulose acetate membrane. The assay involved mixing a culture of sensitive MG1655 cells that carry no resistance against carbenicillin (but carry control plasmids providing kanamycin and chloramphenicol resistance) with the supernatant. Growth of this mixture was monitored by OD measurement. When treated with carbenicillin, only the mixture with supernatant from transporter-expressing cells showed growth of sensitive cells (Fig. S1*C*). The assay was also repeated on hard agar containing carbenicillin (Fig. S1*D*), wherein sensitive cells plated onto the agar form clear growth zones around wells filled with supernatant from transporter-expressing cells. The hlyB and hlyD genes from pVDL9.3 were used in plasmid pRTrans (Table S1) for anhydrotetracycline (aTc) -inducible expression of the transporter genes (Fig. S1*E*, secretion test).

We note here that the LuxR homolog SdiA in *Escherichia coli* interacts strongly with the *rhlI* promoter in the RhlR/RhlI system from *Pseudomonas aeruginosa* but has no significant unintended interference with the LuxR/LuxI quorum-sensing (QS) module in our system (10). As shown in Fig. S1*F*, the circuit shows no detectable signal-based leaky activation of BlaMs in the absence of LuxR. Overall, in our circuit (Fig. 1*C*), in the presence of acyl-homoserine lactone (AHL; produced through LuxI or added exogenously), AHL-bound LuxR within cells can activate synthesis of BlaMs (at a cost), which when secreted through the transport complex, provides benefit in the removal of β-lactam 6-APA.

3. QS-Mediated Gene Activation. LuxR and LuxI are QS components from *Vibrio fischeri* (7, 11, 12). To measure QS activation, we used a fluorescent reporter GFPuv under the control of the P_{LuxI} promoter (pluxGFPuv, ColE1, Cm^R) (6). QS was activated through IPTG. LuxR was expressed under the control of $P_{LtetO-1}$. aTc induction was kept constant for all of the experiments.

To measure QS activation, overnight cultures were diluted at different levels (10^3- to 10^6-fold) in media with 1 mM IPTG (to activate LuxI expression); 200 μL replicates of these cultures were laid out in 96-well microplates (Corning), 50 μL mineral oil were added to prevent evaporation, and the plate was incubated in the plate reader (Victor3; Perkin-Elmer) at 30 °C. Absorbance at 600 nm (OD) and GFP fluorescence (CW lamp filter = 485 nm, emission filter = 535 nm, counting time = 0.1 s) were measured every 10 min with periodic shaking (5 s fast orbital shaking followed by a 5-s pause). As shown in Fig. S2*A*, GFP expression (normalized per cell) follows the same density-dependent path

independent of the initial culture density, an important property of QS-mediated regulation.

To modulate QS activation through expression of LuxI, overnight grown cells were diluted 10^4-fold in media with different levels of IPTG and cultured as before. Increasing IPTG increases signal synthesis, leading to earlier activation visible as higher expression at any given density (Fig. S2*B*).

4. Estimating $3OC_6HSL$ Concentration in QS Population at High Density. As a reference for the strategy to produce the exoenzyme always at a high rate (ON), we estimated the AHL concentration reached by the QS population at a high density (Fig. S2*C*). Cells carrying the full circuitry (pExoI and pRTransp) produce the AHL inducer in the presence of IPTG. These cells, when grown in the absence of IPTG, do not produce the inducer and provide the appropriate base media for building an AHL calibration curve. As a reporter of inducer concentration, we used MG1655 cells with plasmids constitutively expressing LuxR and GFPuv under promoter P_{LuxI} (carrying the same antibiotic resistance as the QS population) (6). Single clones were grown overnight (final OD ~ 0.35 for both) in 2 mL TBK media. The next morning, the cells were diluted 100-fold in TBK media; 200-μL cultures of cells with 50 μL mineral oil were then grown in a 96-well plate, and the OD was monitored. Twelve replicate wells were used for QS culture (with 1 mM IPTG); 72 wells were used for the inducer-free base media (without IPTG). At a sufficiently high OD (~0.15), where high QS activation is clearly observed, incubation was stopped, and the cultures were extracted carefully (180 μL from each well) to avoid mineral oil. Both cultures were centrifuged and sterile-filtered (using 0.2-μm filters) to extract supernatant. Overnight culture (OD ~ 0.5) of reporter cells was diluted 20-fold into both the supernatants. Supernatant from QS culture mixed with the reporter cells was laid out in triplicate (200 μL) in a 96-well plate. To build the calibration curve, the inducer-free base media mixed with the reporter cells was first split into 12 aliquots in 1.5 mL microcentrifuge tubes (1 mL each). Inducer made in TBK media (*Materials and Methods*) was added at the 12 different concentrations indicated; 200-μL cultures from each of these tubes were laid in triplicate with 50 μL mineral oil, and the plate was incubated with shaking for ~12 h, after which time the cultures ware analyzed by flow cytometry. For each well, mean reporter expression was estimated from the cytometry data. Values reported are the geometric mean and SDs from the triplicate wells. The plot of the reporter expression profile shows that QS population had an inducer level of ~9 nM at the cutoff density (Fig. S2*C*). This inducer level was then used as the activation level for the ON state.

5. Mathematical Model of Exoenzyme Dynamics. ***5.1. Population growth.*** We model bacterial growth using the logistic equation (Eq. **S1.1**)

$$\frac{dN}{dt} = gN(1-N), \qquad \textbf{[S1.1]}$$

where N is cell density C (cells/mL) normalized to the carrying capacity of the medium N_M (cells/mL), and g is the specific growth rate (hours^{-1}). Bacterial growth is affected by both the presence of antibiotic and the cost of exoenzyme synthesis. Here, we consider a simplistic relationship (Eq. **S1.2**):

$$g = Benefit - Cost. \qquad \textbf{[S1.2]}$$

We model benefit as the increase in growth rate caused by degradation of the antibiotic (Eq. **S1.3**):

$$Benefit = b_0\frac{b_m}{b_m + Ab}. \qquad \textbf{[S1.3]}$$

b_0 is the maximum growth rate in the absence of any antibiotic and with no enzyme production, b_m is the antibiotic concentration at which growth rate is half-maximal, and Ab the antibiotic concentration.

We assume cost to increase directly with activation E (where $E \in [0,1]$ is the fraction of maximal activation) of exoenzyme production (Eq. **S1.4**):

$$Cost = c_pE. \qquad \textbf{[S1.4]}$$

Here, growth rate is reduced by both antibiotic presence and production cost, and we assume an additive relationship between them.

The cost function may also be replaced with a nonlinear dependence (13) of the form $Cost = \frac{(c_pE)}{\left(1-\frac{E}{E_{max}}\right)}$, where cost increases rapidly as activation reaches an effective level E_{max}. The change to a nonlinear form, however, does not qualitatively change the results shown.

5.2. Exoenzyme synthesis and secretion. Consider a single cell of intracellular volume V_c in the population of density C with maximal exoenzyme production rate k_p. We assume that passive diffusion of enzymes across the cell membrane is negligible and that they are actively secreted by pumps with first-order rate constant D_p. For simplicity, we assume that the exoenzyme degrades with a rate d_p in both the intracellular and extracellular environments. Assuming a well-mixed system, the equations for exoenzyme P can be written as (Eq. **S1.5**)

$$\frac{dP_i}{dt} = k_pE - D_pP_i - d_pP_i \qquad \textbf{[S1.5]}$$

and (Eq. **S1.6**)

$$\frac{dP_e}{dt} = \frac{D_pP_i}{\frac{1}{CV_c}} - d_pP_e, \qquad \textbf{[S1.6]}$$

where i and e indicate exoenzyme concentrations inside the cell and the microenvironment, respectively. D_p is the exoenzyme transport rate constant. $\frac{1}{CV_c}$ captures the dilution of the exoenzyme concentration (D_pP_i) after secreted. Antibiotic Ab degradation is modeled as (Eq. **S1.7**)

$$\frac{dAb}{dt} = -d_{Ab,p}P_eAb - d_{Ab}Ab. \qquad \textbf{[S1.7]}$$

$d_{Ab,p}$ is the rate constant for active degradation of antibiotic by exoenzyme. We model that the antibiotic itself degrades with a low first-order rate constant d_{Ab}.

5.3. QS-based control of exoenzyme synthesis. Based on previous work (14), we model the activation properties of QS with the dimensionless metric v. Density-dependent activation of exoenzyme synthesis under the control of a QS system with potential v can be written as (Eq. **S1.8**)

$$E = \frac{v^a}{\left(\frac{1}{CV_c}\right)^a + v^a}, \qquad \textbf{[S1.8]}$$

where a is the cooperativity of the activation system. v conveys, in multiples of the bacterium volume V_c, the size of the per-cell microenvironment required for half-maximal QS-based activation.

5.4. Positive feedback. Many QS systems are regulated by positive feedback (15), which can be modeled by assuming that signal synthesis rate increases linearly with its own concentration (with an appropriate feedback rate parameter). This model is an approximation of feedback behavior observed in QS, and it is valid for bacterial systems where a graded increase in signal synthesis is observed with signal concentration (16, 17). In previous work (14), we show that this results in an additive relationship between the feedback parameter and signal synthesis, and therefore, the effect of positive feedback can largely be captured as a QS system that activates at a lower density (higher v) than one without positive feedback. The same holds true for other types of QS systems as well, such as where the extracellular signal concentration is detected by cell surface-based reporters. Thus, insofar as the assumption is valid, the effect of positive feedback can be equivalent considered from the perspective of a QS system with a higher v.

5.5. Growth and the effect of cell density. To compare growth of ON and the strategy to not to produce the exoenzyme (OFF) populations (Fig. 1*E*), we numerically solved Eqs. **S1.1–S1.7** by setting activation at $E = 1$ for ON and $E = 0$ for OFF, with all other parameters kept the same. To compare QS, ON, and OFF strategies simultaneously (Fig. 2*A*), we numerically solved Eqs. **S1.1–S1.8** by setting $v = 10^4$ for QS, $v = 0$ for OFF, and $v = \infty$ for ON. In Fig. 2*B*, the simulations were repeated at varying initial densities, and at each time point, the cell density ratio of QS against OFF or ON (whichever was higher) was plotted for comparison. The parameters used in the simulations are listed in Table S2. Typical values were chosen for bacterial cell volume V_c, maximal growth rate b_0, and carrying capacity of medium N_M. Antibiotic was assumed to be relatively stable in media until degraded by exoproduct, and an inherent decay rate d_{Ab}, 100-fold lower than the rate for exoproduct degradation rate d_p, was chosen. Remaining parameters were manually chosen to qualitatively capture the major growth characteristics observed experimentally. The density-dependence of benefit and in turn, the optimality of QS are intrinsic features of this exoenzyme secretion scenario that arise when cost and benefit parameters are significant and comparable (low 6-APA level in our study). These same features can be shown in other scenarios as well, such as with exoenzymes that generate nutrients from available substrates in the environment (14). As such, changes in parameter values change the quantitative aspects of the dynamics shown but do not change the conclusions drawn.

6. QS Advantage Across Different Initial Densities and Lifecycle Times. To examine the specific scenarios where QS is not optimal, we simulated growth of QS, ON, and OFF populations across different values for three parameters: stress level, initial density, and sensing potential. The results show two scenarios, each scenario lasting over a very short time window, during which QS (over a specific potential range) is not optimal (Fig. S4). The first scenario (OFF > QS) occurs because of the inherent delay between the start of exoproduct production and the realization of its benefit (Fig. S4*A*). Although cost is incurred immediately during production, the beneficial reduction in antibiotic requires the dynamical processes of transport and enzymatic reaction, which are not instantaneous. This result leaves a small time window during which QS-controlled activation results in slower growth compared with OFF that does not incur any cost. This time window shortens as v is decreased but being inherent to the dynamics of the process, cannot be completely eliminated by tuning v. We discuss this result in more detail below.

The second, less frequent scenario (ON > QS) occurs when a high-density population is exposed to high stress (Fig. S4 *B* and *E*). Under QS control, production is gradually activated with growth, whereas for the ON case, activation is immediate. To a population already at sufficiently high density at the onset of high stress, immediate activation of exoproduct production can be advantageous. In this scenario, a QS system with a low sensing potential (late activation) is not favorable against ON. As expected, this region is eliminated when a QS system with high v is considered (Fig. S4 *C* and *F*). Barring the above two exceptions, in general, QS emerges as the best control strategy. Furthermore, the simulations show that QS may be tuned appropriately to maximize the region over which it is advantageous, depending on the stress level. In the system shown, the intermediate v represents the optimal QS characteristics, being advantageous or nonlosing in most cases (Fig. S4 *A* and *D*).

7. Cost–Benefit Dynamics in Exoproduct Production and the Optimal Control Strategy. Here, we determine the optimal exoenzyme production rate E_{opt} for bacteria starting growth from low population density in the presence of antibiotic.

Consider the logistic growth equation for a population (Eq. **S1.1**): $\frac{dN}{dt} = gN(1-N)$, where N is cell density (C; cells per milliliter) normalized with respect to the carrying capacity (N_M; cells per milliliter). The specific growth rate (g; 1 per hour) depends on exoproduct production, secretion, and its effect on antibiotic concentration, and simply maximizing it throughout the growth period cannot be used to determine E_{opt}. The reasoning can be elaborated as follows: because antibiotic is added at the start and is not continuously maintained (no steady-state antibiotic concentration), the history of antibiotic concentration becomes a governing factor.

Mathematically, the change in antibiotic concentration Ab can be written as (Eq. **S2.1**)

$$Ab(\tau) - Ab_0 = \int_0^{\tau} \left(\frac{dAb}{dt}\right) dt, \qquad \textbf{[S2.1]}$$

where Ab_0 is the initial concentration of antibiotic in the environment, and $Ab(\tau)$ is the antibiotic concentration after time τ.

Consider the growth of OFF cells ($E = 0$) at time t (Eq. **S2.2**):

$$g_{E=0} = b_0 \frac{b_m}{b_m + Ab(t)}. \qquad \textbf{[S2.2]}$$

Assuming the antibiotic is stable by itself and degrades very slowly in the absence of the exoproduct, we write (Eq. **S2.3**)

$$g_{E=0} = b_0 \frac{b_m}{b_m + Ab_0}. \qquad \textbf{[S2.3]}$$

Now, we consider the case where, at time t, cells that were initially OFF begin to produce exoproduct ($E > 0$) (Eq. **S2.4**):

$$g_{E>0} = b_0 \frac{b_m}{b_m + Ab(t)} - c_p E. \qquad \textbf{[S2.4]}$$

Comparing Eqs. **S2.3** and **S2.4** for change in growth rate by exoproduct production gives us (Eq. **S2.5**)

$$\Delta g_E = b_0 b_m \left(\frac{1}{b_m + Ab(t)} - \frac{1}{b_m + Ab_0}\right) - c_p E. \qquad \textbf{[S2.5]}$$

From Eq. **S2.5**, we note that the extent of reduction in antibiotic concentration ($Ab(t)$ vs. Ab_0) determines Δg_E. However, there is an inherent time lag between exoproduct production and its secretion followed by antibiotic degradation (Eqs. **S1.7** and **S2.1**). Thus, given an exoproduct where coefficients and intermediate reaction rate are finite, $\Delta g_E < 0$ immediately after production until benefit from antibiotic degradation is realized. The time window during which this result occurs depends on the kinetics of enzyme synthesis, secretion, and degradation. The faster these steps, the smaller the time during which OFF > ON.

The above analysis shows that simply maximizing instantaneous growth rate could rule out scenarios (Fig. 1*E*) where the initial drop in growth pays off with increased growth at a later time. Instead, the cumulative account of production determines the optimal strategy—one that maximizes population size $N_T\left(\int_0^T \left(\frac{\partial N}{\partial t}\right)dt\right)$ at the end of the growth period.

The nature of the equations and history dependence make it difficult to find an analytical solution for E_{opt} that maximizes N_T. However, a closer look at the equations provides some insight into the nature of E_{opt}. Consider the quasisteady state, where exoproduct transport is fast compared with exoproduct production. For any given activation level E, the steady-state exoproduct concentration in the environment can be derived by setting $\frac{dP_i}{dt} = 0$ and $\frac{dP_e}{dt} = 0$, giving (Eq. **S2.6**)

$$P_{i,ss} = \frac{k_p E}{D_p + d_p}\; P_{e,ss} = \frac{CV_c D_p}{d_p}\left(\frac{k_p E}{D_p + d_p}\right). \qquad \textbf{[S2.6]}$$

This dependence of P_e on cell density C underlies the requirement for an optimal strategy to be density-dependent. As $C \to 0$ (for low population density), $P_{e,ss} \to 0$, implying high dilution takes exoproduct concentration in the environment to zero. At this low density, antibiotic concentration would remain relatively unaffected by exoproduct production ($Ab_{C\to 0} \approx Ab_0$). Because exoproduct production is costly, as $C \to 0$, $E_{opt} \to 0$ is the best option. However, exoproduct secretion is beneficial at sufficiently high density (Fig. S3*B*), where E_{opt} is a positive finite value. Thus, to maximize N_T, E_{opt} is a specific density-dependent path, in which the appropriate activation level during T depends on the cell density at any given time as well as the stress level and cost of exoproduct synthesis.

QS provides a physical realization of such a density-dependent path. For a QS system of potential v, this path is given by $E_{QS}(N) = \frac{v^a}{\left(\frac{1}{CV_c}\right) + v^a}$. Tuning the QS system to $v = v_{opt}$ provides the best possible QS-controlled activation path. We note that this optimal QS controlled path may not be the same as E_{opt}, which by itself, may not be physically realizable.

If no density exists where activation is beneficial, $E_{opt} = 0$ is the trivial solution, where OFF always wins (such as the no antibiotic case). Similarly, if cost is negligible compared with benefit, the trivial solution is to produce exoproduct at the highest rate independent of density $E_{opt} = 1$.

8. Stochastic Variation in Initial Density. We made use of the stochasticity generated during extreme dilution to examine its effects on QS benefit. In comparing QS vs. OFF (Fig. 3*D*), overnight culture was first diluted 5×10^7-fold into fresh medium without IPTG. This dilution level gives an appropriate frequency of unseeded wells—from 2 to 6 empty wells per 48 wells (f)—giving a mean seeding density [$\lambda = -ln(f) = 2.57$], corresponding to two to three cells per well. This culture was then split into two; to one-half, 1 mM IPTG (QS) was added, and the other one-half received an equivalent amount of water (OFF). These QS and OFF cultures were then laid out in a 96-well plate (48 wells each). After a 6-h incubation, 6-APA was added to all wells, and the plate was then reincubated as before with periodical monitoring of OD.

To study the effect of stochastic spread on QS benefit, we simulated growth of two QS populations, each consisting of multiple subpopulations, with high and low spread in the initial densities of their subpopulations (Fig. 3*E*). Experimentally, we made use of the fact that higher dilution would result in higher spread compared at any mean population density after growth. We first verified this effect by comparing the growth of two uninduced OFF cultures diluted 5×10^7- and 5×10^6-fold (10-fold lower dilution) in the absence of 6-APA. As expected, higher dilution showed higher spread in growth (Fig. 3*B* and Fig. S6*A*).

The same experiment also showed the time lag between the means of the two dilutions. To fairly compare two QS systems under stress, we needed to add 6-APA at the same mean density for the two populations. From three replicate growth experiments (uninduced, no 6-APA), we saw that the two dilutions had time lags of 2.3, 2.5, and 3 h. Therefore, we adopted a 2-h time delay in addition to 6-APA to the high-dilution culture. With this lower (underestimated) time delay, the density at which 6-APA is added to the high dilution culture will likely be lower but not higher than the density at which 6-APA is added to the low dilution. This result ensures that the effect of spread that we observe (wherein high spread outgrows low spread) is not simply caused by a difference in initial density at the time of 6-APA addition.

The experiment was then carried out at follows. Overnight-grown culture was first diluted in media (TBK with 1 mM IPTG) in two 25-mL tubes (5×10^7- and 5×10^6-fold). The dilutions were then laid out in a 96-well plate (48 wells for each dilution). After about 6 h of incubation, 6-APA was added first to low-dilution wells, and the plate was reincubated. After another 2 h, the plate was removed, and the same 6-APA concentration was added to the high-dilution wells. For both dilutions, the 6-APA used was from aliquots kept frozen before the experiment and thawed for 15 min before addition. The plate was then reincubated, and OD was monitored for a period of 48 h. Results from replicate experiments are shown in Fig. S6*B*. The advantage of the high-spread population over the low-spread one was not always equal. We speculate that the difference arises from an underestimate of the time lag (2 h) that varies with each experiment.

9. Evolution of QS Characteristics and Cheater Invasion. With stress that is constant in magnitude and regular over bacterial lifecycles, the biphasic function defines the landscape for the evolutionary tuning of QS characteristics (13). Here, QS characteristics would be directed to v_{opt}, with which overall growth during the lifecycle is maximal (Fig. 4 *B* and *C*). This notion has been speculated based on the observation that natural QS systems seem to be tuned for their specialized niches (18, 19). Several bacteria carry multiple QS systems controlling different functions. In *P. aeruginosa*, the *las* and *rhl* systems display distinct potentials and are activated hierarchically during growth and control elastase and rhamnolipid secretion, respectively (14, 20). Similarly, *Bacillus subtilis* uses two distinct QS systems (14, 21) with vastly different potentials to tightly regulate competence development and sporulation, consistent with the notion that each one is best-adapted to its function.

Our results show the cost effectiveness, robustness, and tuning of QS as a control strategy for a clonal population (relatedness $r = 1$) (22, 23), and it can provide the minimal requirement for adaptive evolution of QS in bacteria (22, 24). However, additional mechanisms, such as kin selection and population structure, would be required to maintain QS and public good-based cooperation in heterogeneous populations containing cheater cells (Fig. S7) that do not produce exoproducts but benefit from them (23, 25–28). Indeed, events such as dispersal (Fig. 4) have been shown to provide the scenarios for QS and QS-mediated cooperation to be maintained (22, 25, 28, 29).

To capture the presence of cheaters in a QS population, we replaced LuxR in pRTrans with reporter GFPmut3, making the cells incapable of responding to AHL and producing exoenzyme, while simultaneously enabling us to identify cheater cells from QS cells using flow cytometry. These cheaters represent the commonly found cheaters among QS bacteria with mutations in the LuxR-type regulator (signal-blind) (22, 25) or the exoproduct genes themselves (30). In our system, the cost of signaling through LuxI-based AHL production is small compared with the cost of exoenzyme synthesis (Fig. 4*C*, row 1 and Fig. S7 *A* and *B*).

We first examined the growth of pure QS and cheater cells in the presence or absence of 6-APA. Overnight-grown QS and cheater cells were both diluted 10^4-fold (overnight ODs were

indistinguishable) in fresh TBK growth media. In the absence of 6-APA, cheater cells initially grew alongside QS cells but eventually outgrew them at high density after activation of enzyme synthesis at high density (Fig. S7*C*). This finding reflects the cost accrued by QS cells after activation at sufficiently high density as discussed in Fig. 4 (no 6-APA case). In the presence of 6-APA, however, QS-controlled production of enzyme was beneficial, and QS cells outgrow cheaters (Fig. S7*D*).

To observe the invasion of a QS population by cheaters, we measured initial and final ratios after growth of a mixed population in the presence of 6-APA. Using the GFP expression of cheaters (Table S1), cheater proportion was measured by flow cytometry of 10,000 cells (Fig. S7*E*) using a FACSCantoII (BD Biosciences) flow cytometer and visualized in FACSDIVA (BD Biosciences). Total cell count was gated based on forward and side scatter, and the number of GFP-positive events (gating on FITC pulse height) was measured. Mixture proportions were measured after 24 h growth in plate. In each case, 50 μL cell mixture to be analyzed were diluted 100-fold and regrown in TBK media for 6 h along with 50 ng/μL aTc for 3 h before fixing in 1% formaldehyde. To ensure that the experimental growth does not change our measurement of GFP-positive cells by somehow affecting GFP expression, pure cheater cells were studied using the same procedure. About 4% of 10,000 events were classified under flow cytometry dark (false negative), but this fraction remained unchanged before and after growth (in the presence of 6-APA), with no visible difference in the expression level of GFP.

Growth of mixed culture of QS and cheater cells showed a clear increase in cheater fraction (>10%) after 24 h of growth in 6-APA (Fig. S7 *E* and *F*). Taken together, these results (Fig. S7 *C–F*) show the expected effect of public good secretion in the presence of cheaters—cheater cells that do not undertake the cost of exoenzyme synthesis fare worse under stress when by themselves but in a heterogeneous population, are able to take advantage of QS cells that invest in exoenzyme secretion.

1. Chervaux C, et al. (1995) Secretion of active beta-lactamase to the medium mediated by the Escherichia coli haemolysin transport pathway. *Mol Gen Genet* 249(2):237–245.
2. Tzschaschel BD, Guzmán CA, Timmis KN, de Lorenzo V (1996) An Escherichia coli hemolysin transport system-based vector for the export of polypeptides: Export of Shiga-like toxin IIeB subunit by Salmonella typhimurium aroA. *Nat Biotechnol* 14(6):765–769.
3. Broome-Smith JK, Spratt BG (1986) A vector for the construction of translational fusions to TEM beta-lactamase and the analysis of protein export signals and membrane protein topology. *Gene* 49(3):341–349.
4. Kenny B, Haigh R, Holland IB (1991) Analysis of the haemolysin transport process through the secretion from Escherichia coli of PCM, CAT or beta-galactosidase fused to the Hly C-terminal signal domain. *Mol Microbiol* 5(10):2557–2568.
5. Sugamata Y, Shiba T (2005) Improved secretory production of recombinant proteins by random mutagenesis of hlyB, an alpha-hemolysin transporter from Escherichia coli. *Appl Environ Microbiol* 71(2):656–662.
6. Collins CH, Arnold FH, Leadbetter JR (2005) Directed evolution of Vibrio fischeri LuxR for increased sensitivity to a broad spectrum of acyl-homoserine lactones. *Mol Microbiol* 55(3):712–723.
7. You L, Cox RS, 3rd, Weiss R, Arnold FH (2004) Programmed population control by cell-cell communication and regulated killing. *Nature* 428(6985):868–871.
8. Everett MJ, Chopra I, Bennett PM (1990) Induction of the Citrobacter freundii group I beta-lactamase in Escherichia coli is not dependent on entry of beta-lactam into the cytoplasm. *Antimicrob Agents Chemother* 34(12):2429–2430.
9. Sohka T, et al. (2009) An externally tunable bacterial band-pass filter. *Proc Natl Acad Sci USA* 106(25):10135–10140.
10. Lindsay A, Ahmer BM (2005) Effect of sdiA on biosensors of N-acylhomoserine lactones. *J Bacteriol* 187(14):5054–5058.
11. Brenner K, Karig DK, Weiss R, Arnold FH (2007) Engineered bidirectional communication mediates a consensus in a microbial biofilm consortium. *Proc Natl Acad Sci USA* 104(44): 17300–17304.
12. Basu S, Gerchman Y, Collins CH, Arnold FH, Weiss R (2005) A synthetic multicellular system for programmed pattern formation. *Nature* 434(7037):1130–1134.
13. Dekel E, Alon U (2005) Optimality and evolutionary tuning of the expression level of a protein. *Nature* 436(7050):588–592.
14. Pai A, You L (2009) Optimal tuning of bacterial sensing potential. *Mol Syst Biol* 5:286.
15. Ng WL, Bassler BL (2009) Bacterial quorum-sensing network architectures. *Annu Rev Genet* 43:197–222.
16. Kuo A, Callahan SM, Dunlap PV (1996) Modulation of luminescence operon expression by N-octanoyl-L-homoserine lactone in ainS mutants of Vibrio fischeri. *J Bacteriol* 178(4):971–976.
17. Ravn L, Christensen AB, Molin S, Givskov M, Gram L (2001) Methods for detecting acylated homoserine lactones produced by Gram-negative bacteria and their application in studies of AHL-production kinetics. *J Microbiol Methods* 44(3):239–251.
18. Schauder S, Bassler BL (2001) The languages of bacteria. *Genes Dev* 15(12):1468–1480.
19. Jung K (2011) Microbiology: Tuning communication fidelity. *Nat Chem Biol* 7(8): 502–503.
20. Pearson JP, Pesci EC, Iglewski BH (1997) Roles of Pseudomonas aeruginosa las and rhl quorum-sensing systems in control of elastase and rhamnolipid biosynthesis genes. *J Bacteriol* 179(18):5756–5767.
21. Grossman AD (1995) Genetic networks controlling the initiation of sporulation and the development of genetic competence in Bacillus subtilis. *Annu Rev Genet* 29: 477–508.
22. Diggle SP, Gardner A, West SA, Griffin AS (2007) Evolutionary theory of bacterial quorum sensing: When is a signal not a signal? *Philos Trans R Soc Lond B Biol Sci* 362 (1483):1241–1249.
23. West SA, Griffin AS, Gardner A, Diggle SP (2006) Social evolution theory for microorganisms. *Nat Rev Microbiol* 4(8):597–607.
24. Brown SP, Johnstone RA (2001) Cooperation in the dark: Signalling and collective action in quorum-sensing bacteria. *Proc Biol Sci* 268(1470):961–965.
25. Diggle SP, Griffin AS, Campbell GS, West SA (2007) Cooperation and conflict in quorum-sensing bacterial populations. *Nature* 450(7168):411–414.
26. Nadell CD, Foster KR, Xavier JB (2010) Emergence of spatial structure in cell groups and the evolution of cooperation. *PLoS Comput Biol* 6(3):e1000716.
27. Griffin AS, West SA, Buckling A (2004) Cooperation and competition in pathogenic bacteria. *Nature* 430(7003):1024–1027.
28. Chuang JS, Rivoire O, Leibler S (2009) Simpson's paradox in a synthetic microbial system. *Science* 323(5911):272–275.
29. Keller L, Surette MG (2006) Communication in bacteria: An ecological and evolutionary perspective. *Nat Rev Microbiol* 4(4):249–258.
30. Schaber JA, et al. (2004) Analysis of quorum sensing-deficient clinical isolates of Pseudomonas aeruginosa. *J Med Microbiol* 53(Pt 9):841–853.

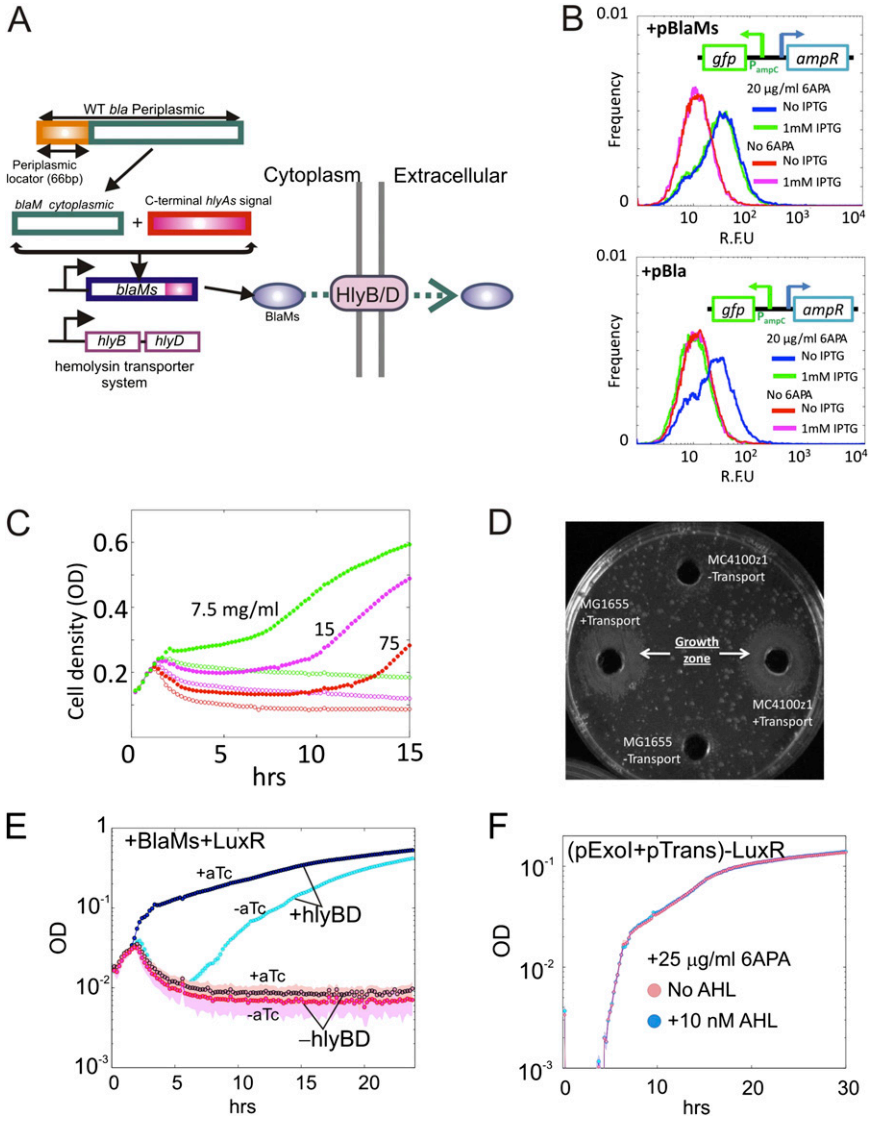

Fig. S1. BlaMs as a secreted exoenzyme to degrade β-lactam antibiotics. (*A*) Schematic of BlaMs construction. BlaM is the mature cytoplasmic form of WT Bla without the N-terminal periplasmic signal peptide. BlaMs is formed by the fusion of BlaM and HlyAs, the C-terminal transport signal sequence from the hemolysin HlyA. The transporter genes *hlyB* and *hlyD*, when expressed, enable the secretion of a protein carrying the HlyAs signal into the extracellular environment. (*B*) Cytoplasmic BlaMs (unlike WT periplasmic Bla) does not prevent cell wall damage from β-lactam antibiotics. P_{ampC} is induced as a result of 6-APA action that causes cell wall damage. We compared the protection against 6-APA provided by BlaMs (*Upper*) with the protection by WT Bla (*Lower*). IPTG was used to induce expression of BlaMs and Bla from plasmids pExo and pBla, respectively. If cytoplasmic BlaMs prevents 6-APA-caused cell wall damage, its expression should decrease the induction of P_{ampC} reported by GFP [relative fluorescence units (R.F.U.)]. GFP expression did not show significant difference between with (green) and without (blue) BlaMs induction, indicating that BlaMs expression did not prevent cell wall damage by 6-APA. Induction of WT *Bla* caused significant decrease in GFP expression to a level that matches basal-level GFP expression (in the absence of 6-APA). As a control, measurements without 6-APA treatment are shown for the cases with (pink) and without (red) 1 mM IPTG. (*C*) Liquid phase test of BlaMs secretion by hlyB-hlyD transporter. Sensitive cells supplemented with supernatant from cells grown with the transporter (filled circles) recovered from β-lactam carbenicillin treatments of indicated concentration, whereas no recovery was seen in the absence of transporters (unfilled circles). (*D*) Solid phase test of BlaMs secretion. Sensitive MG1655 cells from a high-density culture were spread on agar plates containing 5 μg/mL carbenicillin. Holes were made into the agar and filled with supernatant from indicated cell strains grown with pExo with or without transporter in the presence of IPTG. After overnight incubation at 37 °C, only the wells holding supernatant from cells with the transport machinery show clear growth zones corresponding to diffusing BlaMs. (*E*) Testing of aTc-inducible BlaMs secretion by hlyB-hlyD in the synthetic circuit. JM109 cells carried plasmid ptethlyBD (Table S1) (hlyB and hlyD under PLtetO-1) along with a compatible plasmid for constitutive (aTc-independent) BlaMs expression. Supernatant from overnight growth at 30 °C was tested for protection against β-lactam antibiotic as in *A*. (*F*) Control test for luxR function in AHL binding and BlaMs production during growth. JM109 cells carrying pExoI and pTrans (all circuit genes except *luxR*) were treated with 6-APA as in Fig. 1*E*. Presence or absence of AHL made no difference to the growth in contrast with Fig. 1*E* and Figs. S3 and S5, where cells (JM109 carrying pExoI and pRTrans) at high initial density showed initial growth retardation followed by overtake of uninduced cells.

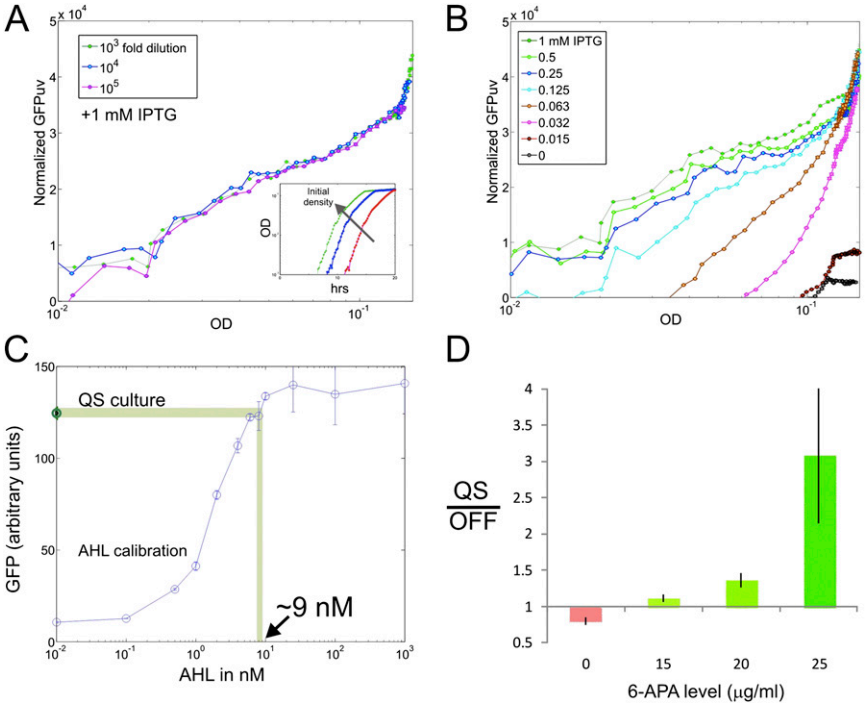

Fig. S2. Density-dependent activation under QS control through AHL based signaling. (*A*) Density-dependent activation (of GFPuv) is independent of initial density. JM109 cells carrying the QS circuitry and the lux-based GFPuv reporter were grown overnight and diluted (10^3-, 10^4-, and 10^5-fold) to different initial densities (shown in different colors) in the presence of 1 mM IPTG to activate the QS circuit for LuxI production. Normalized GFP expression was calculated from subtracting GFP reading of blank TBK (~2,900 counts) and dividing by corresponding OD_{600} subtracted for blank TBK (0.042). Dots indicate mean values, and error bars indicate SD from four replicate measurements. Showing the density-dependent target gene activation under QS, GFP expression follows the same density-dependent path independent of the initial culture density. (*Inset*) Growth curves of the corresponding three dilutions. (*B*) Increasing IPTG (LuxI production) shows shift in activation to lower density; 10^5-fold diluted culture was grown with indicated IPTG levels. Normalized GFP expression calculated as in *A*. (*C*) Estimation of AHL level in high-density culture. Blue points show reporter expression at indicated inducer concentration. Brown circle on the vertical axis marks the observed reporter expression from the JM109 cells (carrying pExoI and pRTrans) that overlaps the calibration around 9 nM. Error bars for all points are from three replicates. (*D*) Benefit of exoenzyme production increases with increase in 6-APA. Adapted from Fig. 4*C*, this figure compares QS (1 mM IPTG) with OFF at varying 6-APA levels. In each case, the ratio was taken when either QS or OFF reached a high OD at 0.13. Error bars are propagated values from four replicates.

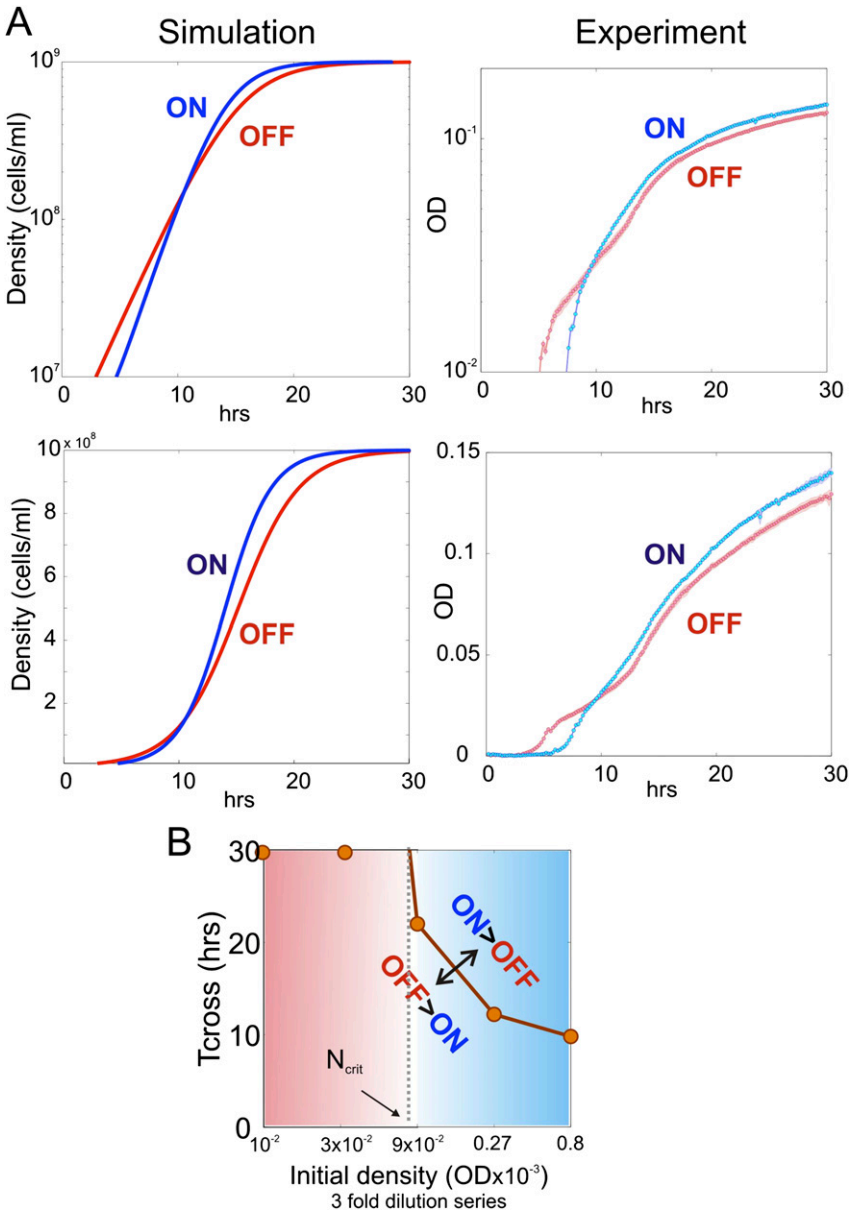

Fig. S3. Cell density determines benefit of production. (*A*) Rescaled versions of Fig. 1 *D* and *E* for comparison of ON and OFF growth starting at high initial density. (*Right*) The data are shown in log scale (*Upper*; smaller density range than originally shown in the text) and (*Lower*) linear scale. Each dot represents the average from three technical replicates, and the shaded area spans the SD. (*Left*) Corresponding simulation results. (*B*) Measured *Tcross* for different initial densities. At each initial density, *Tcross* indicates the time when the means of ON and OFF growth curves crossed. At the lowest initial densities, no cross-over was observed during the growth period. The shading from pink to blue indicates the transition from a low-initial density region, at which ON cannot outgrow OFF, to a high-density area, where ON can outgrow OFF given time *Tcross*. We mark *Ncrit* in this approximate transition region. Initial densities (OD) values were calculated from the OD measurement of the overnight culture and the dilution level.

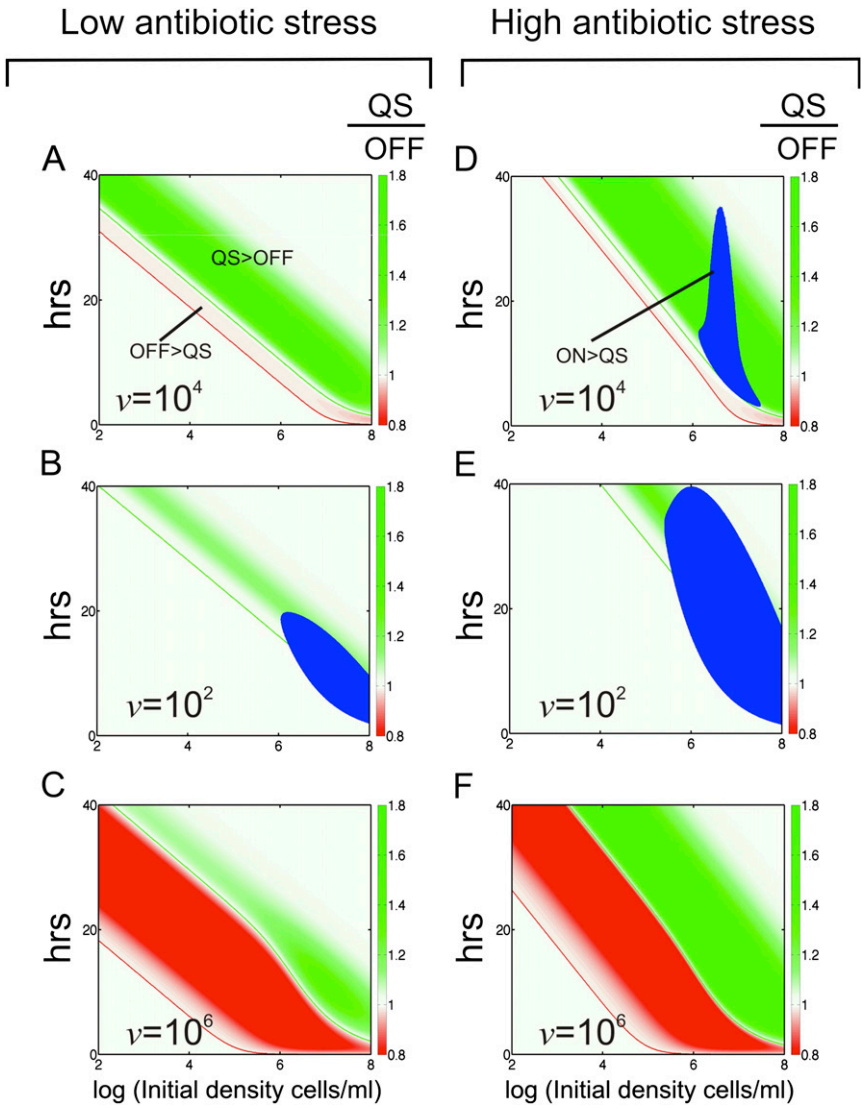

Fig. S4. Comparing different QS systems across stress levels, Simulations comparing ON, OFF, and QS were carried out with QS systems that activate at an intermediate density ($v = 10^4$ in *A* and *D*), high density ($v = 10^2$ in *B* and *E*), or low density ($v = 10^6$ in *C* and *F*) for low (100) and high (200) antibiotic concentration. The definition of sensing potential *v* as a metric for QS-mediated activation is in the text. The intensity of the color (red to green) indicates the ratio of the density reached by QS and OFF at any given time. Colored lines are shown to help demarcate the scenarios where a particular strategy is best. To demarcate the regions, a difference of 1% in cell density at any point was considered significant. Moving along the diagonal from left to right (*A*), the red line indicates transition from QS = OFF to OFF > QS. The next transition occurs at the green line, where QS > OFF. The blue area covers the region where ON > QS. With low $v = 10^2$ (*B* and *E*), production occurs later in growth, and the time window where OFF > QS is reduced (not visible at this scale); correspondingly, the area where ON is the best strategy increases. With high $v = 10^6$ (*C* and *F*), production occurs early during growth (at lower density), where higher dilution increases the time window in which OFF > QS. v_{opt} would be an intermediate value (as seen with $v = 10^4$ in *A* and *D*) that maximizes the area. The interplay continues at higher antibiotic level, but the relative areas occupied by QS, ON, and OFF are now different, suggesting a different v_{opt}. This interplay of the optimal QS characteristics is seen in Fig. 4.

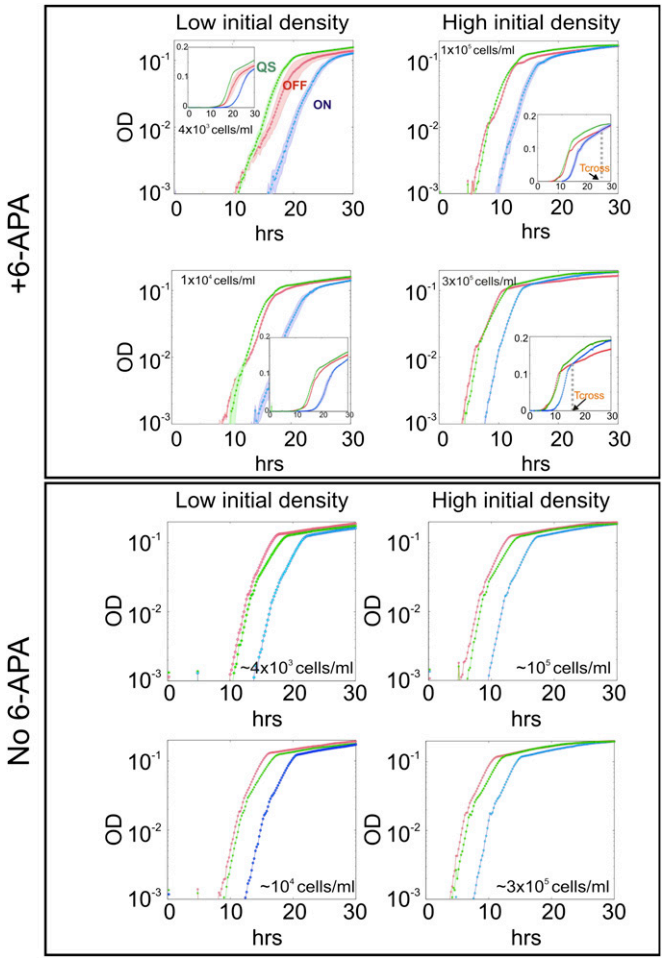

Fig. S5. Density-dependent activation through QS. (*Upper*) QS-mediated regulation is advantageous in the presence of 6-APA, regardless of initial density. Growth of QS, ON, and OFF populations starting from the indicated low (*Left*) and high (*Right*) initial densities in the presence of 25 μg/mL 6-APA. *Insets* show the corresponding results in linear scale to highlight the cross-over of ON and OFF indicated by the vertical stippled line. Each data point is the average of four replicates, and the shaded area spans the SD. Initial densities (cells per milliliter) were estimated from the dilution level and density of the overnight culture. (*Lower*) QS-mediated regulation is not advantageous in the absence of 6-APA. Figures show growth of QS, ON, and OFF populations (as discussed in *Upper*). In the absence of any stress, OFF is always the best strategy, whereas ON is always the losing strategy.

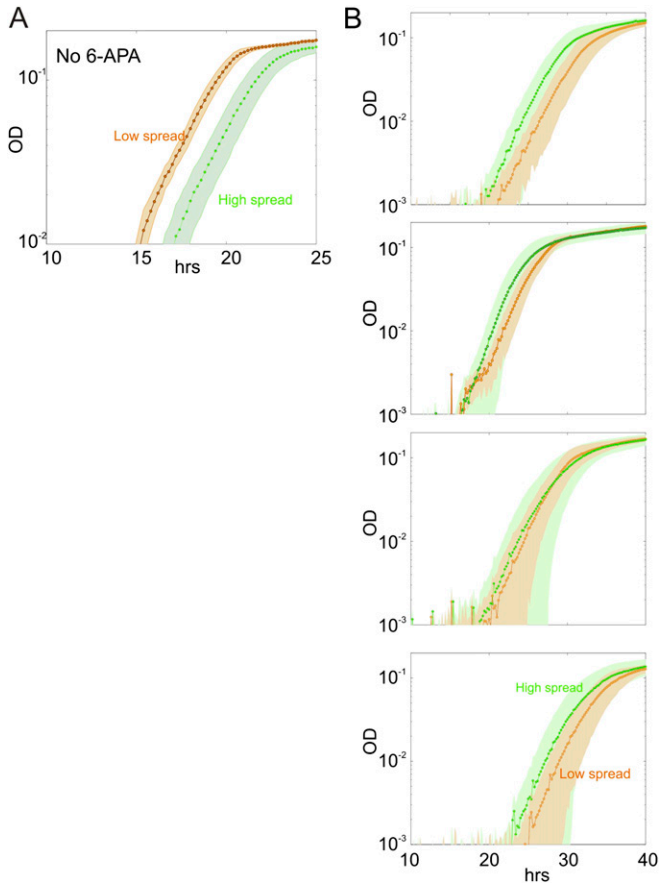

Fig. S6. Growth dynamics under Poisson dilution. (*A*) Higher dilution generates higher spread. Growth of high (5×10^7-fold) and low (5×10^6-fold) diluted uninduced (OFF) populations in the absence of 6-APA. The higher spread (green) in the high-dilution case over the low-dilution case (orange) case is visible. The two growth curves showed a time lag of 2.3 h between them. Each dot is averaged over 48 wells, and the shaded area captures the SD. (*B*) Results from four additional replicate experiments (in addition to Fig. 3*F*) comparing growth of QS populations under high and low dilution in the presence of 6-APA.

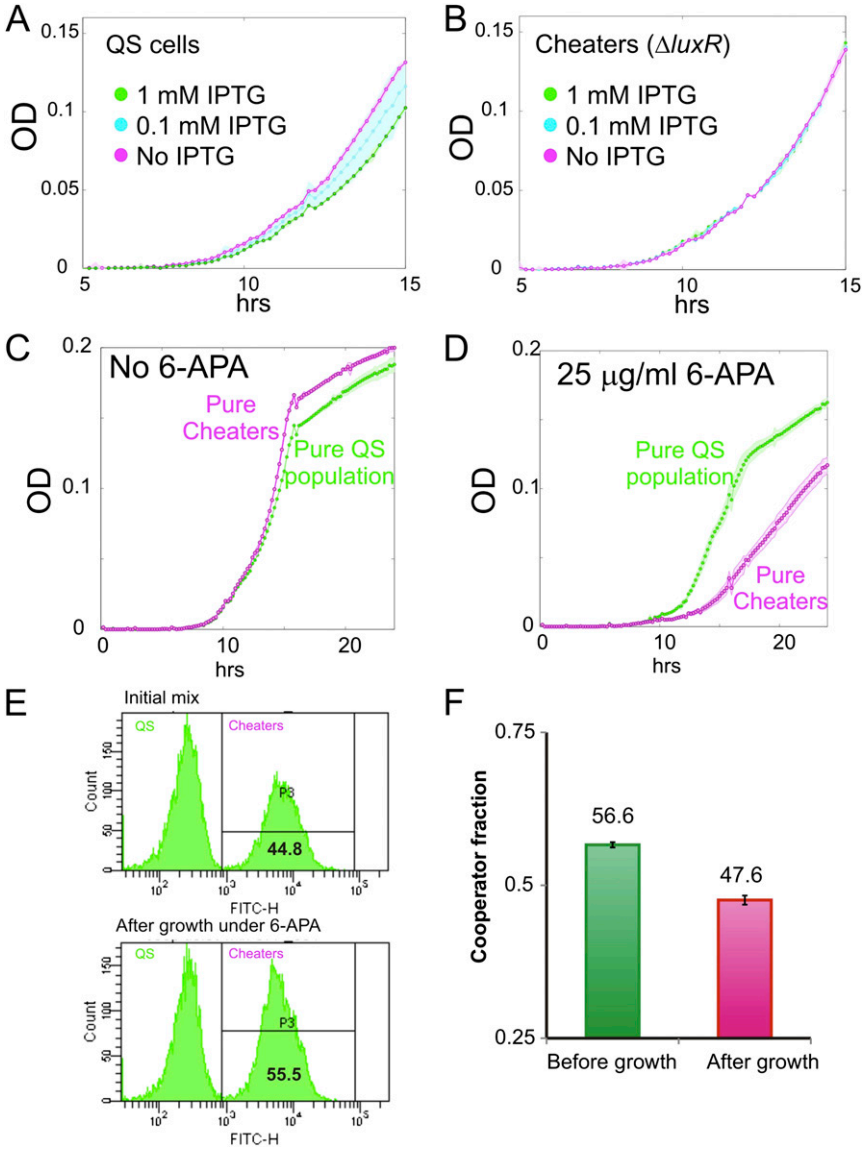

Fig. S7. Cost of LuxI production under IPTG is negligible compared with cost of exoproduct synthesis and cheater invasion in the public goods scenario. (*A* and *B*) Growth curves of QS (*A*) and cheater cells (*B*) grown separately under indicated IPTG levels in the absence of 6-APA are shown. Cheater cells lack LuxR (carrying pGFPTrans instead of pRTrans) but are, otherwise, similar to QS cells; both QS and cheater cells carry IPTG-inducible LuxI. Increasing IPTG in the absence of 6-APA reduces growth for QS cells, which incurs cost of exoenzyme synthesis when activated at sufficiently high density but gets no benefit. IPTG has no effect on the cheater cells. Each dot is averaged over four replicates, and the shaded area spans the SD. (*C* and *D*) Growth of pure QS (green) and cheater (magenta) population in the absence (*C*) and presence (*D*) of 6-APA. (*E*) Typical flow cytometry results used for estimating proportion of QS and cheaters before and after growth. (*F*) Invasion of QS cells by cheaters. Percentage of QS cells in mixture of QS and cheaters measured before the start of experiment and after 24 h growth under 25 μg/mL 6-APA. Error bars shown are from five replicates.

Table S1. List of plasmids used in the study

Plasmid name	Origin and selection marker	Description
pPROlar.A122	p15a, Kan	Base vector for cloning; IPTG controls expression of genes from hyrbid $P_{lac/ara-1}$ promoter (1)
pBlaM	p15a, Kan	Intermediate plasmid for cloning, expression of cytoplasmic BlaM
pExo	p15a, Kan	IPTG controls expression of BlaMs from $P_{lac/ara-1}$ promoter
pExoI	p15a, Kan	AHL $3OC_6HSL$-inducible expression of BlaMs in the presence of LuxR; IPTG controls expression of LuxI
pluxRI	p15a, Kan	IPTG controls expression of LuxR and LuxI; QS controlled expression of GFPuv when paired with plasmid pluxGFPuv
pluxR	p15a, Kan	IPTG controls expression of LuxR; used as detector for inducer $3OC_6HSL$ when paired with plasmid pluxGFPuv
pVDL9.3	sc101,Cm	Expression of transporter genes under the P_{lac} promoter (2)
pPROTetE	colE1,Cm	Base vector for aTc-inducible gene expression (Clontech)
ptethlyBD	colE1,Cm	aTc-inducible promoter, $P_{LtetO-1}$, for expression of transporter genes; repressor TetR constitutively expressed from P_{laclq} promoter
pRTrans	colE1,Cm	aTc-inducible promoter, $P_{LtetO-1}$, for expression of transporter genes and LuxR; repressor TetR constitutively expressed from P_{laclq} promoter
pGFPTrans	colE1,Cm	aTc-inducible promoter, $P_{LtetO-1}$, for expression of transporter genes and GFPmut3 and repressor TetR constitutively expressed from P_{laclq} promoter; complementary to pRTrans as cheater plasmid
pluxGFPuv	colE1,Cm	Reporter GFPuv under P_{LuxI} promoter to observe QS activation (3)

1. Chervaux C, et al. (1995) Secretion of active beta-lactamase to the medium mediated by the Escherichia coli haemolysin transport pathway. *Mol Gen Genet* 249(2):237–245.
2. Tzschaschel BD, Guzmán CA, Timmis KN, de Lorenzo V (1996) An Escherichia coli hemolysin transport system-based vector for the export of polypeptides: Export of Shiga-like toxin IIeB subunit by Salmonella typhimurium aroA. *Nat Biotechnol* 14(6):765–769.
3. Broome-Smith JK, Spratt BG (1986) A vector for the construction of translational fusions to TEM beta-lactamase and the analysis of protein export signals and membrane protein topology. *Gene* 49(3):341–349.

Table S2. Model parameters

Parameter	Units	Description
V_c	1×10^{-15} L	Intracellular volume of an average *E. coli* cell
N_M	10^9 cells/mL	Carrying capacity of growth medium
E	0–1	Fractional activation of exoproduct production
k_p	100 nM h^{-1}	Maximum intracellular exoproduct production rate on full activation
D_p	100 h^{-1}	Transport rate constant of exoproduct from intracellular to extracellular space
d_p	0.1 h^{-1}	Inherent decay rate of β-lactamase protein
Ab_0	0–200 units	Initial antibiotic concentration
$d_{Ab,p}$	0.5 $unit^{-1}$ μM^{-1} h^{-1}	Active β-lactamase catalyzed degradation of antibiotic
d_{Ab}	0.001 h^{-1}	Inherent decay rate of antibiotic; assumed to be relatively stable by itself
b_m	100 units	Antibiotic concentration at which growth rate is half-maximal
b_o	0.75 h^{-1}	Benefit parameter representing the maximal growth rate
c_p	0.25 h^{-1}	Cost parameter for (fractional) reduction in growth rate at maximal activation
a	1–2	For the *luxR*, *luxI* system from *V. fischeri*, we take a = 1.6 (1)

1. Kenny B, Haigh R, Holland IB (1991) Analysis of the haemolysin transport process through the secretion from Escherichia coli of PCM, CAT or beta-galactosidase fused to the Hly C-terminal signal domain. *Mol Microbiol* 5(10):2557–2568.